JOURNAL OF APPLIED PHYSICS 111, 000000 (2012)

Thickness driven stabilization of saw-tooth–like domains upon phase transitions in ferroelectric thin films with depletion charges

I. B. Misirlioglu,[a] H. N. Cologlu, and M. Yildiz
Faculty of Engineering and Natural Sciences, Sabanci University, Tuzla/Orhanli, Istanbul 34956, Turkey

(Received 5 October 2011; accepted 4 February 2012; published online xx xx xxxx)

Ionized impurities have nearly always been neglected in discussing the limit of functionality of ferroelectric thin films. One would certainly expect that the thickness limit for functionality would be altered in the presence of ionized impurities, but how this would occur remains unclear. In this article, we analyze the domain structures as well as the phase transition temperatures in films with depletion charges for various film thicknesses. Depletion charges induce a position-dependent built-in field that leads to an inhomogeneous distribution of ferroelectric polarization. Such an inhomogeneity in the polarization results in strong depolarizing fields in films. We show that formation of saw-tooth–type domains is a way to circumvent the depolarizing fields, even in films with ideal electrodes. There is a critical film thickness above which the saw-tooth domains develop. On the other hand, the phase transition of the ultrathin structures with electrodes having a finite screening length, namely real electrodes, is always into the multidomain state during cooling from the paraelectric state, regardless of the presence of depletion charges. An important finding we have is that the transition temperature in films with real electrodes does not depend nearly at all on the depletion charge density unless it is very high ($>10^{26}$ ionized impurities/m^3). Relatively thick films (>8 nm in this work) with real electrodes that have very high depletion charge densities have transition temperatures very similar to those with the same charge density, but with ideal electrodes, making us conclude that thick films with high depletion charge densities will hardly feel the finite screening effects. The results are provided for (001) $BaTiO_3$ films grown on (001) $SrTiO_3$ substrates with pseudomorphic top and bottom metallic electrodes. © *2012 American Institute of Physics*. [http://dx.doi.org/10.1063/1.3691938]

I. INTRODUCTION

The intrinsic limit of ferroelectricity in thin films has been a topic of extensive discussions in many reports. A strained, planarly confined, thin ferroelectric (FE) structure exhibits dramatic changes in the dipole configurations commensurate with strong deviations from bulk states. One fact is that the formation of defects, such as ionic vacancies, interstitials, and dislocation networks, are inevitable, owing to both the process conditions and the developing strains in the film on misfitting substrates during fabrication. The defect fields and their impact on the physical properties of FEs both in bulk and film form have been the focus of numerous studies, including dedicated book chapters.[1–14] It has been well understood that the vacancy or impurity-type point defects lead to a depletion zone upon formation of the metal-film contact during electroding. The motivation to study such material systems has been to understand the limit of existence of ferroelectricity as a function of thickness and electrode-interface conditions, particularly focusing on depolarizing field effects.[15–25] A recent study, for example, based on a first principles approach, reports that a possible asymmetry in the material type for the top-bottom film electrode contacts could compete with the depolarizing effects through an internal bias field and reduce the critical thickness of a switchable ferroelectric polarization's existence to about two unit cells.[26] Besides applications in nano-scale memory devices, field effect transistors, and tunable layers in integrated circuits,[4,24,27] these materials have also become a test bed in the past few decades for studying phase transitions and critical behavior in the solid state, probably only second to magnetic materials.

Fabrication of these systems in capacitor geometries naturally results in the equilibration of the chemical potential at the metal-ferroelectric interfaces in ferroelectric films that often have impurity states, and the formation of a charged region on the film side is nearly inevitable. This has been mostly analyzed experimentally in addition to a few theoretical studies,[11,28–31] including attempts in artificially graded structures.[32] As will be shown, the depletion charge itself acts as a source of inhomogeneity and the situation is not very different from introducing compositional gradients to the system. Recently, several works have been devoted to especially understand the evolution of these charges under limited lattice diffusivities, but how such phenomena will be impacted by size effects remain an important aspect to be understood.[33,34] Furthermore, it is well known that charged defects, such as impurities and vacancies, will be quite immobile at temperatures near room temperature (RT) and might get populated at interfaces and defect sites probably only after several thousands of applied field cycles.[7,35]

In a real ultrathin ferroelectric film, due to the very short distances at which potential drops occur, it becomes very

[a]Author to whom correspondence should be addressed. Electronic mail: burc@sabanciuniv.edu.

© 2012 American Institute of Physics

Author Proof

crucial to elaborate the interaction between depletion charges and the consequences of the extent of screening at the film-electrode interface. Film thicknesses at the order of a few tens of nanometers are comparable to the depletion zone widths expected in ferroelectric films, with metallic electrodes inducing a depletion potential of around 1 V. For typical densities of impurities (between 10^{24} and 2×10^{26}) we consider in this paper, we estimate depletion widths of around 100 nm to around 8 nm at each electrode interface. As the total of these depletion width values at each interface are quite close to the film thickness ranges of interest in our work, we assume fully depleted films when stated, particularly when finding the phase transition temperatures. The discussion on the effect of partial depletion on the domain structures is an exception to the full depletion assumption, but we show that the two situations are not very different for films not thicker than 28–30 nm. Depletion widths of around 30 nm and ionized impurity densities of around $10^{25–27}/m^3$ have been reported by Pintilie *et al*. using interfacial capacitance measurements for $PbZr_{0.2}Ti_{0.8}O_3$ films.[36,37]

The attempts to clarify the depletion charge effects have mostly been confined to very simple charge distributions as analysis of realistic distributions, even when depletion charge density is homogeneous, via analytical approaches can become a formidable problem. Only a few studies exist that try to analyze the effects of continuous depletion charge distributions on the observable properties in relatively thick films[7,38–41] but these studies have considered the single domain states. The possibility that, due to the inhomogeneous nature of the system owing to depletion charges, the transition could be into multidomain states even in structures with ideal electrodes would make a prominent difference in the calculated transition temperatures, which is one of the main emphases given in this paper. The way in which phase transition characteristics would be altered is discussed rigorously by Bratkovsky and Levanyuk[29] in the absence of dead layers. Reduction in the critical temperature commensurate with smaller coercivities in the ferroelectric state was demonstrated along with a qualitative discussion on the possibility of domain formation. One could easily foresee that the conclusions withdrawn for systems with ideal electrodes will have to be modified, for instance, for systems that have imperfect film-electrode interfaces, namely real electrodes. The real electrodes with finite Thomas-Fermi screening can be modeled as a thin dead layer between the electrode and the FE film, as demonstrated by Bratkovsky and Levanyuk in their 2009 paper (See Ref. 29). This latter statement is indeed a very important one when discussing experimental results on ferroelectric stability in the light of electrostatic considerations.

In this article, we address the question as to whether or not depletion charge effects could compete and overwhelm dead layer effects due to conditions at the film-electrode interfaces. To probe the competing energies, we use the Landau-Ginzburg-Devonshire (LGD) formalism for ferroelectric materials coupled with the interface conditions and presence of depletion charges. Firstly, films of various thicknesses with perfect film-electrode interfaces, namely ideal electrodes, but with depletion charges, are analyzed. A saw-tooth–type domain structure forms in relatively thick films due to the inhomogeneous internal field. At the transition temperature, thick films with ideal electrodes, but high depletion charge density always exhibit the saw-tooth domains. The period of this domain structure grows with increasing film thickness. Following this analysis, we introduce thin dead layers at the film-electrode interfaces to find out the possible alterations to the domain configurations and sensitivity of the domains to thickness effects. We found out that the domain period in a film having dead layers is altered upon introduction of a homogeneous depletion charge density to the system. At high depletion charge densities, domains with a saw-tooth type structure develop regardless of the presence of the dead layers. We also show that the transition temperatures are significantly lowered in relatively thick films with high depletion charge densities and dead layers, while this lowering is minimal in the thinner films and remain nearly unchanged with respect to charge-free films with dead layers. This behavior is a direct consequence of the dead layer effects dominating at low thicknesses, while thicker films are under a heavier influence of depletion charges. Our results reveal the magnitudes of changes that can be expected in the transition temperatures for films with depletion charges, considering, especially, the transition into multidomain states.

II. THEORY AND METHODOLOGY

In this section, we give the governing equations and boundary conditions used to obtain field- and temperature-dependent characteristics of the ferroelectric thin film capacitors. The schematic of the geometry considered is given in Fig. 1. A two-dimensional grid is constructed that has $200n \times kn$ cells, where $k(n)$ is the number of cells along the film thickness (width) and each cell has a dimension of 0.4 nm, nearly the lattice parameters of well-known pseudo-cubic perovskites, such as $BaTiO_3$ (BT), to imitate the order of lengths at which P can vary in the system compared to real systems. Polarization is obtained by solving the equations of state derived from the LGD free energy for all P in our system for an epitaxial monodomain (001) BT

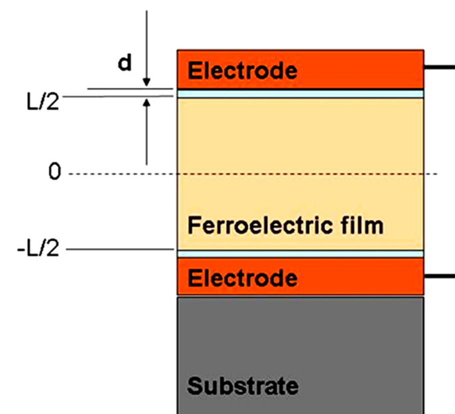

FIG. 1. (Color online) The schematic of the ferroelectric capacitor considered in this study.

Author Proof

ferroelectric film on a (001) $SrTiO_3$ cubic substrate along with the Maxwell equation for dielectric displacement, employing a finite difference discretization. The strain states of the films determine the stable P components. We partition the thin film capacitor system along the thickness axis, z, as follows:

$$w=1 \quad \text{when} \quad -h/2 \leq z \leq +h/2, \quad w=0 \quad \text{when} \quad -h/2-d<z<-h/2 \quad \text{and} \quad +h/2 < z < d+h/2, \tag{1}$$

where w is a step-wise function defining the interface between the dead layer and the ferroelectric, d is the dead layer thickness (taken as 1-unit cell-thick, ~0.4 nm in this work), and $|h|$ is the thickness of the ferroelectric layer. The electrode-dead layer interfaces are at $-h/2-d$ and $d+h/2$, respectively. Note that $d=0$ indicates the absence of a dead layer, i.e., a perfect film-electrode contact interface. The equations of state for the system to define the relation between the fields in the layers and the P components as well as ε_r of the dead layers using the definition of w in Eq. (1) are

$$w\left[2\alpha_3^m P_3 + 4\alpha_{13}^m P_3 P_1^2 + 4\alpha_{33}^m P_3^3 + 6\alpha_{111} P_3^5 + \alpha_{112}(4P_3P_1^4 + 8P_3^3P_1^2) + 2\alpha_{123}P_3P_1^4 - G\left(\frac{\partial^2 P_3}{\partial z^2} - \frac{\partial^2 P_3}{\partial x^2}\right)\right] + (1-w)\frac{D_3}{\varepsilon_r\varepsilon_0} = wE_3^F + (1-w)E_3^d, \tag{2a}$$

$$w\left[2\alpha_1^m P_1 + 2(2\alpha_{11}^m + \alpha_{12}^m)P_1^3 + 2\alpha_{13}^m P_1 P_3^2 + 6\alpha_{111}P_1^5 + 2\alpha_{112}[3P_1^5 + 3P_1^3P_3^2 + P_1P_3^4] + 2\alpha_{123}P_1^3P_3^2 - G\left(\frac{\partial^2 P_1}{\partial z^2} + \frac{\partial^2 P_1}{\partial x^2}\right)\right] + (1-w)\frac{D_1}{\varepsilon_r\varepsilon_0} = wE_1^F + (1-w)E_1^d, \tag{2b}$$

where P_i ($i=1,3$) are the components of P in the ferroelectric state, α_3^m, α_{13}^m, α_{33}^m, α_1^m, α_{11}^m, and α_{12}^m are the renormalized dielectric stiffness coefficients modified by the misfit strain and the two-dimensional clamping of the film, while α_{111}, α_{112}, and α_{123} are the dielectric stiffness coefficients in the bulk,[42] and $\boldsymbol{G}$ is the gradient energy coefficient and is assumed to be isotropic for convenience with a value of 3×10^{-10} m^3/F. E_3^F, E_1^F and E_3^d, E_1^d are the fields along the z- and x-axis in the ferroelectric layer and the dead layer, respectively. The equality between the field and the dielectric displacement in the dead layer (**w = 0**) reads

$$D_3 = \varepsilon_r\varepsilon_0 E_3^d \quad \text{and} \quad D_1 = \varepsilon_r\varepsilon_0 E_1^d \tag{3}$$

and, for w = 1 (ferroelectric layer),

$$D_3 = \varepsilon_b\varepsilon_0 E_3^F + P_3 \quad \text{and} \quad D_1 = \varepsilon_b\varepsilon_0 E_1^F + P_1. \tag{4}$$

The dead layer, when present, is assumed to be a high-k dielectric, whose dielectric constant, ε_r, is 20 to exemplify its effects and ε_b is the background dielectric constant of the ferroelectric (taken as 7 in this work[43]). The electric fields in both the ferroelectric layer and the dead layer are computed from the gradients of the electrostatic potential from

$$E_3^F = -\frac{\partial\phi^F}{\partial z}, \quad E_1^F = -\frac{\partial\phi^F}{\partial x} \tag{5}$$

for the ferroelectric and

$$E_3^d = -\frac{\partial\phi^d}{\partial z}, \quad E_1^d = -\frac{\partial\phi^d}{\partial x} \tag{6}$$

in the dead layers, with ϕ^F and ϕ^d being the electrostatic potential in the ferroelectric and the dead layer, respectively. The electrostatic potential in each layer can be found at each point as a function of P and the dielectric constant of the dead layer using the Maxwell relation in the absence of free charges $\nabla\cdot\hat{\boldsymbol{D}}=0$ and $\nabla\cdot\hat{\boldsymbol{D}}=\rho$ when depletion charges due to ionized impurities are present. ρ is the volumetric charge density (0 when no impurities are present). Thus, one has

$$\frac{\partial^2\phi^F}{\partial z^2} + \frac{\partial^2\phi^F}{\partial x^2} = \frac{1}{\varepsilon_b\varepsilon_0}\left(\frac{\partial P_3}{\partial z} + \frac{\partial P_1}{\partial x} - \rho\right) \tag{7}$$

in the ferroelectric layer and

$$\frac{\partial^2\phi^D}{\partial z^2} + \frac{\partial^2\phi^d}{\partial x^2} = -\frac{\rho}{\varepsilon_r\varepsilon_0} \tag{8}$$

for the dead layer. We assume that each impurity contributing to ρ has only one positive unit charge (the charge of one electron) in all cases. The depletion charge density in this work, both in full and partial depletion cases, is assumed to be constant throughout the film volume, which is indeed realistic enough, especially for thicknesses at the order of a few tens of nanometers (See Refs. 30, 36, and 37), where full depletion is possible. The boundary conditions we employed for $P_{1,3}$ are

$$\left[P_1 + \lambda\frac{\partial P_1}{\partial z}\right]_{z=-\frac{h}{2},\frac{h}{2}} = 0, \quad \left[P_3 + \lambda\frac{\partial P_3}{\partial z}\right]_{z=-\frac{h}{2},\frac{h}{2}} = 0, \tag{9}$$

Author Proof

J_ID: JAP DOI: 10.1063/1.3691938 Date: 16-March-12 Stage: Page: 4 Total Pages: 10

PROOF COPY [JR11-7191R] 124205JAP

at the top and bottom electrode-film interface of the ferroelectric, where the extrapolation length, λ, is taken as infinite. Periodic boundary conditions are used along the x-axis, i.e.,

$$P_3(z, x=0) = P_3(z, x=L), P_1(z, x=0) = P_1(z, x=L). \tag{10}$$

We apply Dirichlet boundary conditions in the electrostatic equations to solve P in the thin film capacitors. At the dead layer-electrode interfaces, $-h/2 - d$ and $h/2 + d$ ($d = 0$ corresponds to ideal electrodes), $\phi = 0$ corresponds to short-circuit boundary conditions between the electrodes. Figure 1 shows the geometry adopted. Note that the entire "capacitor system" is neutral as the charges from ionized impurities, whose density is ρ, accumulate on the electrodes, and, thus, the number of positive and negative charges are equal.

Equations of state [Eqs. (2a) and (2b)] along with the equations of electrostatics in [Eqs. (7) and (8)] using relations given in Eqs. (3) and (6) are solved simultaneously for P components employing a Gauss-Seidel iterative scheme subject to boundary conditions mentioned above in Eqs. (9) and (10). The simulations always start with small fluctuations of z and x components of P around zero that later on develop into the domain structure, depending on dead layer and film thickness. We limit ourselves to 10 000 iterations converging to a difference of about 10^{-8} between consecutive iterative P solution steps when ferroelectricity exists. Owing to the compressive in-plane misfit in (001) $BaTiO_3$ on (001) $SrTiO_3$ (about 2.5%), only P_3 is the spontaneous polarization that, in addition to when depletion charge exists, also contains the built-in polarization, P_b. Thus, from here onwards, the ferroelectric part of P_3 will be denoted as P_f and the built-in part as P_b. Note that, when $\rho = 0$, there is only one solution and it is $P_3 = P_f$.

III. RESULTS AND DISCUSSION

A. Room temperature domain structures when $d = 0$ (ideal electrodes)

We start discussing our results for three different film thicknesses, 12 nm, 16 nm, and 20 nm, with perfect film-electrode interfaces obtained at room temperature (RT), assuming that these films are fully depleted (Part of our results are also given in Ref. 44). This assumption can be justified by noting that, for instance, in the case of impurity densities around 10^{26}, one might expect depletion zone thickness of around 8–10 nm, depending on the dielectric constant attaining values around 100–200 in a typical ferroelectric at room temperature, which indicates a total depletion zone of 16 to 20 nm for a film with top and bottom electrodes if the interfaces are symmetric. Structures with depletion charge at the max density limit considered in our work (2×10^{26} ionized impurities/m^3) that are thinner than 10-nm thickness are nearly always found to exist in an imprinted single domain state and are not of interest here. The reason for this outcome is discussed in the proceeding paragraphs. The films without any depletion charge also exist in a homogeneous monodomain state and are not discussed here again for brevity. In general, throughout this work, we chose to study two different depletion charge densities that reflect moderate-high and very high impurity densities reported for such structures. Depletion charge densities as high as 10^{25-27} ionized impurities/m^3 were reported,[31] and we remain around these (5×10^{25} ionized impurities/m^3 for the moderate-high limit and 2×10^{26} for the high limit) values in our simulations.

Figure 2 displays the domain structures that form in films of various thicknesses that have a fixed volumetric depletion charge density corresponding to 2×10^{26} ionized impurities/m^3. Upon finding that low densities of depletion charge yield only a unidirectional P_f in thin films, we focus on the densities that do trigger domains in thick structures (>10 nm). As a comparison, for example, the 8-nm-thick film with the aforementioned depletion charge density (2×10^{26} ionized impurities/m^3) does not undergo a domain stabilization, owing to the "insufficient extent of inhomogeneity", meaning it is not thick enough for the built-in field to render a highly inhomogeneous structure considering full depletion. By inhomogeneous, we mean here the dependence of the local Curie temperature on the built-in electric field at that location. Extremely high densities of depletion charge (>10^{27} ionized impurities/m^3) could perhaps stabilize domains in thicker films (>28 nm) with ideal electrodes, but are out of the main scope of our study.

In Fig. 2, we give the total polarization along with the ferroelectric polarization, and the latter is obtained by subtracting P_b from P_3 for 12 nm, 16 nm, and 20 nm films. The P_b is found by running our calculations above the Curie point, as it is nearly temperature insensitive and is the only corresponding solution satisfying Eqs. (2a), (7), and (8) [please see Fig. 3(a) for P_b when full depletion is assumed for a 20-nm film]. At 2×10^{26} ionized impurities/m^3, a saw-tooth–type domain pattern develops at RT, whose period is a function of thickness. Relatively lower depletion charge densities (<10^{26} ionized impurities/m^3) do not tend to stabilize domains and result in a uniaxial P_f whose amplitude is less in one half of the film than in the other half, concomitant

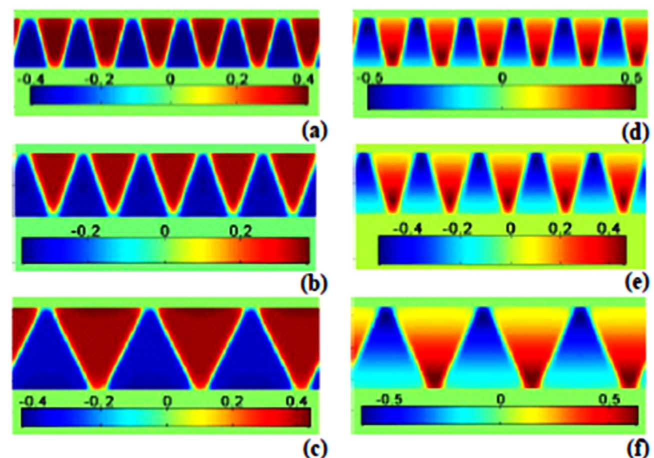

FIG. 2. (Color online) The RT domain total polarization configurations of the (a) 12-nm, (b) 16-nm, and (c) 20-nm-thick films with 2×10^{26} ionized impurities/m^3 (on the left-hand side) and the extracted ferroelectric polarization given for (d) 12-, (e) 16-, and (f) 20-nm-thick films on the right-hand side. Scales are given to display the range of P_3 in C/m^2.

Author Proof

ID: satheeshkumaro Time: 12:42 I Path: Q:/3b2/JAP#/Vol00000/120628/APPFile/AI-JAP#120628

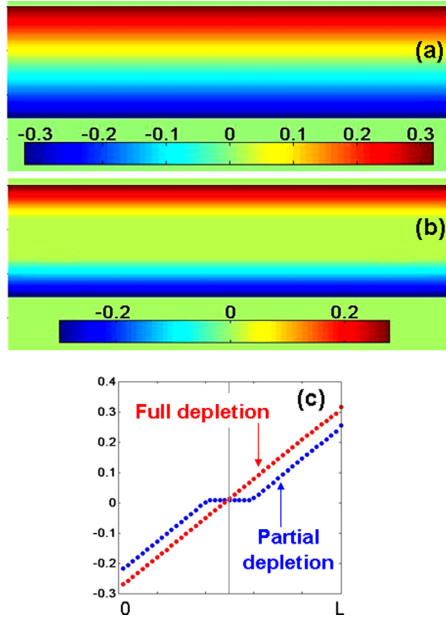

FIG. 3. (Color online) Schematic of the built-in field plotted as a function of position along the thickness of the ferroelectric film for a 2×10^{26} impurity/m^3 charge density in the case of (a) full depletion, (b) partial depletion, and (c) comparison of the built-in polarization along the thickness of full and partial depletion cases.

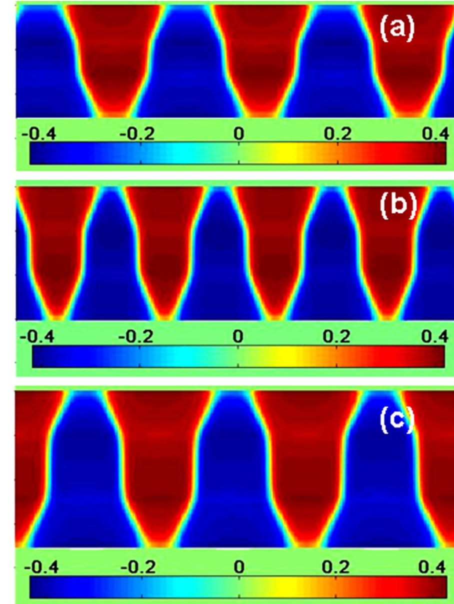

FIG. 4. (Color online) Domain structures in the case of (a) 20-nm, (b) 24-nm, and (c) 28-nm-thick films for partial depletion consideration for a 2×10^{26} impurity/m^3 charge density. The depleted layers are 8-nm-thick into the film starting from the film-electrode interfaces.

361 with the internal field distribution. Therefore, the formation 362 of domains in thicker films is due to the highly inhomogene- 363 ous nature of the built-in field renormalizing the linear term 364 in P_3 in Eq. (2a). Here, the amplitude of the variation in the 365 local transition temperature naturally becomes more pro- 366 found toward the film boundaries, with increasing thickness 367 for a given constant charge density. The situation described 368 that applies to our analysis is also schematically depicted in 369 Figs. 3(a)–3(c) for clarity. Hence, thicker structures are 370 forced to undergo domain stabilization to minimize the depo- 371 larizing fields emanating from the gradient of the polariza- 372 tion induced by the inhomogeneous built-in field. The 373 domain period in such a high inhomogeneous system 374 becomes a function of position, somewhat similar to what 375 has been reported for discrete, artificially graded structures,[45] 376 where the authors calculated domain fractions.

377 Those results reveal that the domain structures forming 378 due to the depletion charge–induced fields in systems with 379 ideal electrodes is quite different from what occurs when 380 dead layers are present. For instance, in the latter, ferroelec- 381 tric polarization amplitude attains a maximum in the middle 382 section of the film, while saw-tooth–type domains have the 383 maximum amplitude of the ferroelectric polarization wave 384 near the electrode interfaces.

385 We find it important to add that, for depletion zone 386 widths smaller, but comparable to film thickness where a 387 charge-free region exists, we still see a similar behavior to a 388 fully depleted film. P_b in the case of partial depletion is pro- 389 vided in Figs. 3(a)–3(c) for a 20-nm film with 8 nm depletion 390 at each interface. If one carries out a more complete deple- 391 tion width, w_d, calculation within the assumption that the 392 ionized impurities have a constant density in the depletion 393 zone using

$$w_d = \left[\frac{2\varepsilon_0\varepsilon_r(\phi_d - \phi_a)}{N_d q}\right]^{1/2} \tag{11}$$

395

396 for a dielectric constant of the ferroelectric (ε_r) being at the 397 order of 200 and for the number of ionized impurities around 398 2×10^{26}/m^3, one finds that depletion width starting from the 399 electrode-film interface is about 8 nm in the film. In Eq. (11), 400 ϕ_d and ϕ_a are the depletion potential (or barrier from the 401 metal side) and external applied potential, respectively, (zero 402 when discussing w_d in this formulation). Domain structures 403 far below the transition (room temperature) for the afore- 404 mentioned partial depletion in the case of a 20-nm-thick film 405 is provided in Fig. 4. For the full-depletion assumption, we 406 had found that a saw-tooth–type domain configuration is sta- 407 bilized. For a 20-nm-thick film, this would mean that there is 408 a depleted region having a thickness of 2×8 nm = 16 nm at 409 the interfaces, with a charge free region in the middle sec- 410 tion. Our calculation shows that the saw-tooth domain struc- 411 ture is still present despite the charge-free region in the 412 middle of the film, as given in Fig. 4 for 20-nm, 24-nm, and 413 28-nm-thick films. This behavior is quite straightforward to 414 justify: The domains emanating at the interfaces where a 415 strong built-in field exists do now want to terminate in the 416 charge-free middle section with either a head-to-head or a 417 tail-to-tail domain configuration, which is energetically 418 costly. Moreover, the domain walls in the charge-free middle 419 section are perpendicular to the film plane to minimize the 420 total energy. In films with thickness being equal to or smaller 421 than $2 \times w_d$, the situation converges to full depletion, already 422 analyzed in this work.

423 For sufficiently thick films with high impurity density, 424 the depletion zone in the film will be confined to a relatively 425 small volume near the electrodes and the entire film could be

Author Proof

free from saw-tooth–type domains existing in a single domain state. Moreover, in the case of low impurity density and thicker films ($2 \times w_d \cong t$, where t is film thickness), a domain-forming built-in field might not be expected, but the built-in field will shift the hysteresis along the field axis and smear the transition anomalies, as demonstrated in a previous work,[39] as well as reducing the Curie temperature.

B. Room temperature domain structures when $d = 1$ (dead layers present)

In the presence of dead layers ($d = 1$ unit cell) and depletion charge, a competition between the two formations, each of which is a source of inhomogeneity, takes place. Here, we focus on fully depleted films with dead layers. A set of structures at RT for three different thicknesses and two depletion charge densities are provided in Fig. 5. The left-hand side gives the domain structure in the absence of depletion charge, while the right-hand side is when depletion charge is present. Subtracting the P_b at each site from P_3, we again get the P_f, as we did in Subsection III A. Among the analyzed structures, relatively moderate density of depletion charge (5×10^{25} ionized impurities/m^3 in this work) slightly alters the domain wall angles with respect to the film normal along with a period change, as will be discussed next. A charge density of 2×10^{26} stabilizes the saw-tooth domain structure that has the prominent maxima in the P_f profile at the domain tips, similar to the case when $d = 0$. Such a formation indicates that thick films with high depletion charge densities are under "weaker influence" of the dead layers. Another effective way to enable the comparison of the domain periods in films with and without depletion charge for a given thickness would be to plot and discuss the wave vector k of domains ($k = 2\pi/\lambda$, where λ is domain period) as a function of thickness, as we do in the preceding paragraphs.

Before discussing the probable changes in domain period when depletion charges are present in thin films, we give the results for the domain wave vector, k, we obtained both in our simulations and using the approach presented in Ref. 46 to validate the trends of our simulations for charge-free films in Fig. 6(a). A summary of the approach in Ref. 46 in a modified form (see also Ref. 47) is given in the Appendix for convenience. Our numerical results are in excellent agreement with the results obtained using the methodology in the Appendix, confirming the reliability of the method. Note the approach in the Appendix adopted from Refs. 46 and 47 analyzes the phase transition point, considering linear equation of state. We find that the domain period does not nearly change at all with further cooling upon the transition from the paraelectric to the multidomain FE state and transforms from a sinusoidal pattern to a square-like one, making it feasible to compare k values at and below the transition. In other words, even when our simulation temperatures are not the same as the

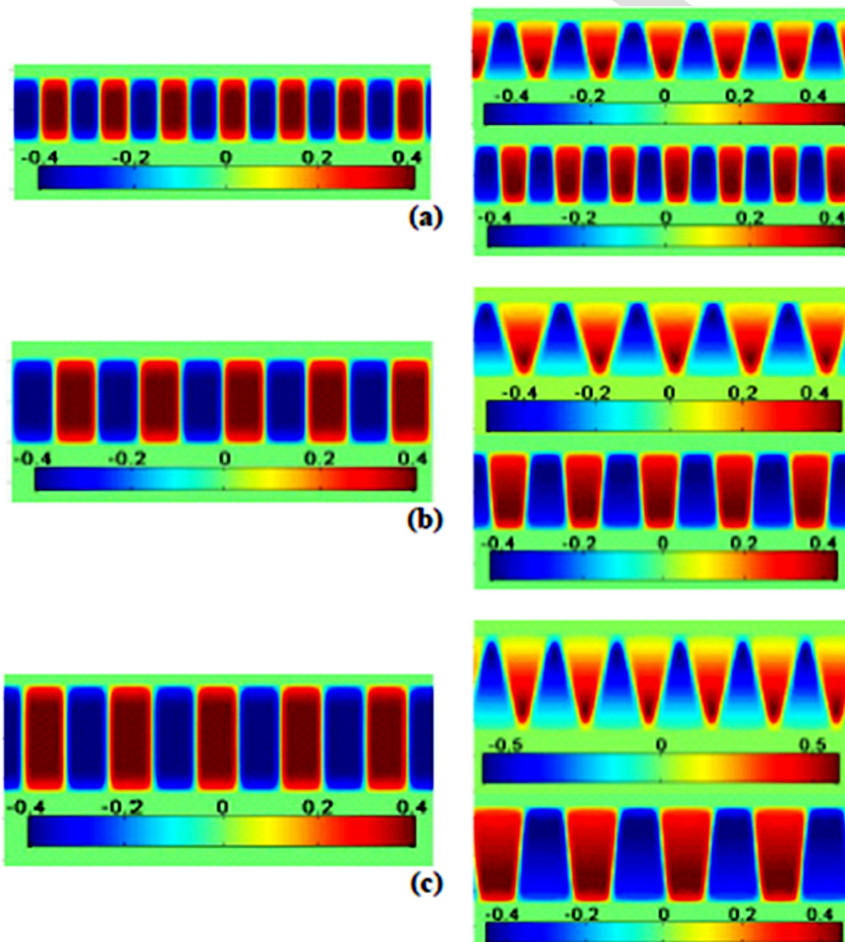

FIG. 5. (Color online) Domain structures for (a) 12-nm, (b) 16-nm, and (c) 20-nm-thick films with dead layers. On the left-hand side are the domain structures for 0 impurity density and $d = 1$. The right-hand side of each color map for a given thickness are the domain structures for impurity densities of 5×10^{25} (upper color map) and 2×10^{26} (lower color map). Scales are given to display the range of P_3 in C/m^2.

478 temperatures at which the k values were found using the
479 approaches in Refs. 46 and 47, the k's in both their study
480 and our simulations are directly comparable.
481 To visualize the impact of depletion charge on the do-
482 main structures in films with dead layers, we now discuss
483 behavior of the wave vector, k, of the P_f wave plotted as a
484 function of film thickness for ionized impurity densities of
485 5×10^{25} and 2×10^{26} /m^3. Our results for films at RT with-
486 out and with depletion charge are in Fig. 6(b). The presence
487 of electrical domains in films with depletion charge has per-
488 sisted for the entire thickness range of interest in our study.
489 Domain period for films thinner than 12 nm with 5×10^{25}
490 ionized impurities/m^3 is smaller than the charge-free film,
491 while 2×10^{26} ionized impurities/m^3 follows more or less
492 the charge-free film, but with slightly larger k values (i.e.,
493 smaller domain period). The general trend of the increase
494 in k values for films thinner than 12 nm in our work might
495 be perceived as an indication that the depletion charge
496 amplifies the depolarizing field for a given set of material
497 parameters (domain wall energy, fixed dead layer thickness,
498 dielectric constant, etc.). But this trend changes with

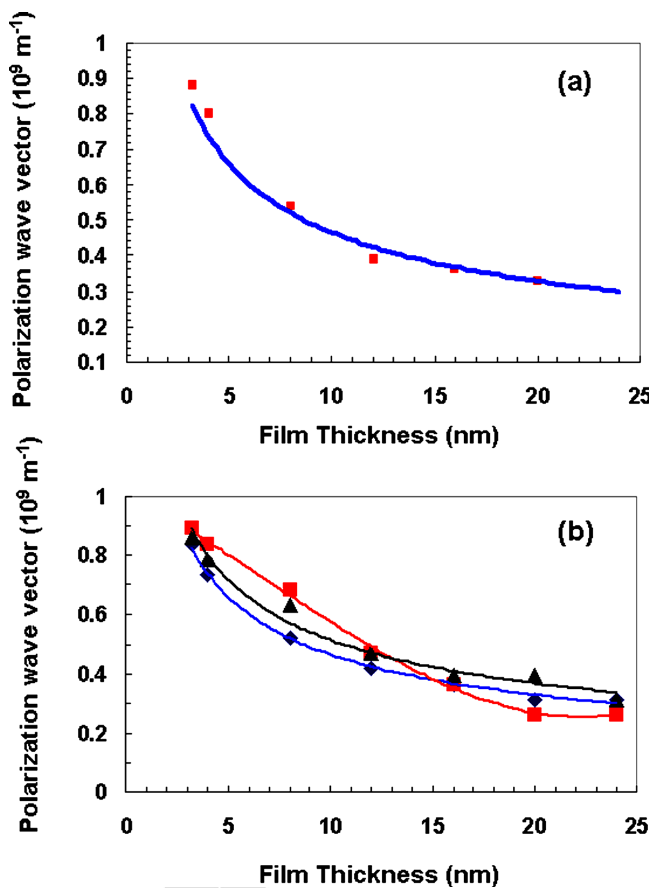

FIG. 6. (Color online) (a) Wave vector of the polarization along the film plane as a function of film thickness at the transition derived from solving Eq. (A16) for the point of loss of stability of the paraelectric phase summarized in the Appendix (solid curve) and the wave vector we found in our simulations (solid squares) for $d = 1$ unit cell. (b) Wave vector of the polarization along the film plane as a function of thickness for films without charge (curve with diamonds), films having 5×10^{25} ionized impurities/m^3 charge density (curve with squares), and films having 2×10^{26} ionized impurities/m^3 charge density (curve with triangles) for $d = 1$ unit cell. The curves in (b) passing through the data points are guides for the eyes.

499 increasing film thickness for the films having 5×10^{25} ion-
500 ized impurities/m^3 with respect to the charge-free case.
501 Around 15 nm, a crossover occurs, after which the thicker
502 films with 5×10^{25} ionized impurities/m^3 carrier density
503 develop a coarser domain structure. Here, from the data of
504 our simulations, we can see that the domain period is
505 altered in a way the depolarizing field appears to be ampli-
506 fied, leading to a finer domain period, hence, a larger k.
507 Still, we cannot arrive at general conclusions for the entire
508 thickness regime we considered, as thicker films (>16 nm)
509 with moderate-high depletion charge density have a dis-
510 tinctly different domain period. Despite the thought that
511 any formation giving rise to or amplifying depolarizing
512 fields will reduce the transition temperature, comparing the
513 k values for a given thickness does not lead us to conclude
514 so. To analyze the effect of depletion charge effects on the
515 transition temperature, we carry out cooling runs in our
516 simulations and extract and discuss the transition tempera-
517 tures in Subsection III C.

C. Phase transition temperatures 518

519 This section considers the case of films where the
520 entire volume is depleted, as we note that a further detailed
521 discussion might be necessary to compare partial depletion
522 and full depletion effects for various impurity densities.
523 Furthermore, for asymmetrical film-electrode interfaces, it
524 is clear that such effects might be altered significantly. We
525 had already mentioned, for symmetrical film-electrode
526 interfaces, that films with high impurity densities, where
527 the depletion zones are confined to the near-electrode
528 region, can exist in a single domain state and the transition
529 temperatures will set accordingly. We leave this compari-
530 son for future work and focus on films with depletion zones
531 being at the order of the film thickness, i.e., full depletion.
532 The paraelectric-ferroelectric transition temperatures for
533 films with full depletion are expected to be lowered in the
534 presence of depletion charges, dead layers, or when both
535 coexist. Film thickness importantly comes into play in all
536 of the cases above (See Figure 7). Here, we emphasize the
537 situation when dead layers and depletion charges are both
538 present, but also run a case where the films at a thickness
539 range of 3.2 nm to 24 nm have ideal electrodes for compari-
540 son. For reference, we first computed the transition temper-
541 ature as a function of film thickness for a fixed dead layer
542 thickness ($d = 1$) and dielectric constant (ε_r = 20) and our
543 results are in Fig. 7(a) along with the results we obtained
544 using the method prescribed in the Appendix. We find the
545 transition temperatures by tracking $\langle|P_3|\rangle$ in our simula-
546 tions. The transition temperatures computed from the nu-
547 merical solution of Eq. (16a) in the Appendix have a very
548 good match with the simulation results presented in this
549 work, again confirming the validity of the prescribed
550 method in Sec. II (Figure 7(a)). It must be borne in mind
551 that the approach of Ref. 45 excludes the gradient of P_3
552 (total polarization) along the thickness of the film, which
553 we do include in our study. This can be the possible cause
554 of the slight deviation between the two results at small
555 thicknesses. As expected, decreasing film thickness results

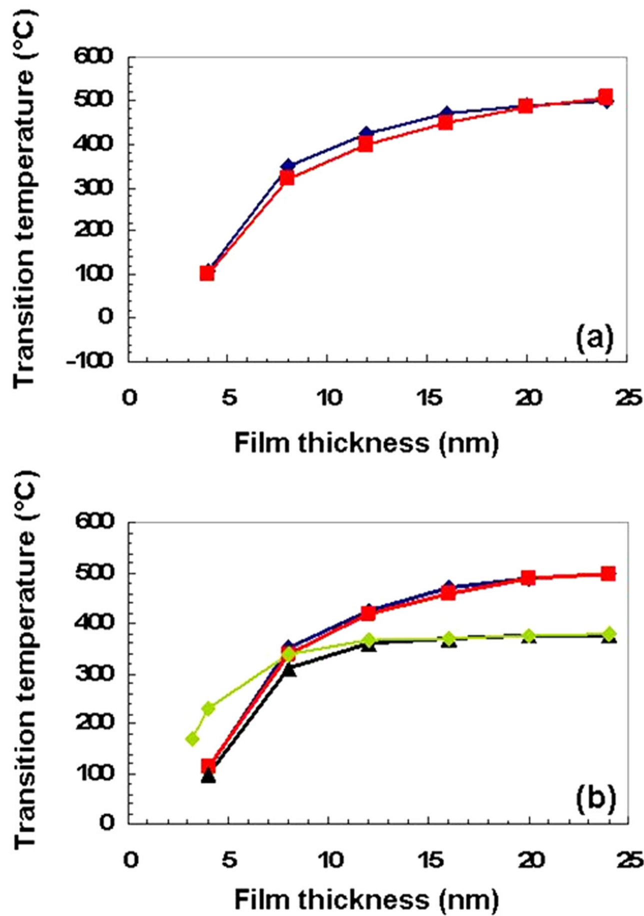

FIG. 7. (Color online) (a) Phase transition temperatures in films with dead layers as a function of thickness when (a) no charge is present. The curve with diamonds is the results of our simulations, and the curve with squares is the results obtained by solving Eq. (A16) in the Appendix after Ref. 43. (b) Comparison of the results for charge-free (curve with diamonds) films having 5×10^{25} ionized impurities/m^3 depletion charge (curve with squares) and films having 2×10^{26} ionized impurities/m^3 depletion charge (curve with triangles), and the curve with triangles is the case for $d = 0$ (no dead layer) and 2×10^{26} ionized impurities/m^3 depletion charge given for comparison. Note that, in (b), the curve with squares and the curve with the solid dark diamonds have a strong overlap, where the latter is just partially visible.

556 in a reduction of the transition temperature, with domain 557 period subsequently becoming comparable or larger than 558 the film thickness. Note that we do not go down to very low 559 temperatures, where ultrathin films (<3.2 nm in this work) 560 might be in a single domain state upon transition from the 561 paraelectric phase and that this takes place at quite low 562 temperatures.

563 Computing the phase transition temperatures in films 564 with dead layers, but now with two different depletion 565 charge densities, we note that films with a charge density of 566 5×10^{25} ionized impurities/m^3 have nearly the same transi- 567 tion temperature compared to the charge free ones for a 568 given thickness [see Fig. 7(b)]. Note that a homogeneous 569 charge distribution does not lead to any net bias fields 570 between the electrodes, and no smearing of the transition 571 exists, meaning the transition temperature is sharp. We then 572 carried out the cooling runs for films having a depletion 573 charge density of 2×10^{26} ionized impurities/m^3 both in the 574 presence and absence of dead layers to detect the transition.

575 As mentioned previously, tracking $\langle|P_3|\rangle$ and comparing it 576 with $\langle P_3\rangle$ allows us to detect the phase transition, if it is into 577 a multidomain state. These films with 2×10^{26} ionized 578 impurities/m^3 and dead layers have a similar trend with the 579 charge-free films at small thickness, but then the transition 580 temperature is significantly reduced for thicker films. More- 581 over, the transition temperatures in thicker films with and 582 without dead layers are nearly the same. This scenario is 583 certainly different for thinner films (<12 nm), and it is seen 584 that the dead layers entirely dominate the transition charac- 585 teristics [compare the curves for the films having 2×10^{26} 586 ionized impurities/m^3 with and without dead layers in Fig. 587 7(b)]. This is solely due to the "degree of induced 588 inhomogeneity" in the thicker films, where the built-in elec- 589 tric field due to depletion charges induce a strong gradient of 590 the transition temperature via normalization of α_3^m in Eq. 591 (2a), causing a larger amplitude variation of P_f, possibly 592 overriding dead layer effects. Therefore, we provide quanti- 593 tative evidence that the thicker films will be under a stronger 594 influence of the depletion charge effects compared to thinner 595 ones. One must remember here, however, that we discuss the 596 case of rather high densities of depletion charge. For moder- 597 ate-to-low densities (<10^{25} ionized impurities/m^3 in this 598 work), the above discussion on transition temperatures 599 merely converges to discussion of dead layer effects on the 600 transition temperature as a function of film thickness.

IV. CONCLUSIONS 601

602 We have analyzed the phase transition characteristics of 603 ferroelectric thin films with and without depletion charge, 604 considering ideal electrodes and film-electrode interface 605 with dead layers. Using the non-linear Landau-Ginzburg- 606 Devonshire equation of state, simulations were carried out 607 for films with different thicknesses at different temperatures 608 to find the domain periodicities and transition temperatures 609 as a function of depletion charge density at various thick- 610 nesses. The approach adopted from Refs. 46 and 47 has been 611 used as a guide to check the validity of our simulation 612 results. (001)$BaTiO_3$ grown on (001)$SrTiO_3$ with pseudo- 613 morphic electrodes was used as an example system. Films 614 with high depletion charges split into saw-tooth–type 615 domains, even when ideal electrodes are present. This hap- 616 pens when the film is above a critical thickness, below which 617 a single domain, imprinted state is stabilized. Increase in 618 film thickness naturally creates larger variations in the elec- 619 tric field, hence, in local transition temperatures, due to a 620 constant density of depletion charge, and a saw-tooth–type 621 domain structure is favored, even in films with ideal electro- 622 des to minimize the depolarizing fields. Partially depleted 623 films, when the depleted volume is comparable to the film 624 volume, could still develop saw-tooth-type domains. The lat- 625 ter happens with the exception that the domain walls are par- 626 allel to the film normal to reduce domain wall energy. 627 Presence of dead layers when depletion charge densities are 628 not very high (<10^{26} ionized impurities/m^3) determine the 629 transition temperature both for thin (<10 nm) and thick films 630 (>10 nm). At charge densities not very high, domain periods 631 are slightly altered, subsequent with tilted domain walls with

Author Proof

respect to domain configurations in charge-free films. Although high charge densities in films with dead layers stabilize saw-tooth–type domains, regardless of the presence of the dead layers, the fact that very thin films (<10 nm) exist in a fine period multidomain state as opposed to what happens in films with ideal electrodes reveals the domination of the dead layer effects in thin films. While transition temperatures of ultrathin films having depletion charge are set by the dead layers, high depletion charge densities (2×10^{26} ionized impurities/m^3 in this work) dominate over dead layer effects in thicker films. This can be judged by comparing the very similar results for these films with and without dead layers, i.e., the relatively thicker films with high depletion charge densities and dead layers have identical transition temperatures as those with the same depletion charge density, but ideal electrodes.

ACKNOWLEDGMENTS

I.B.M. has been partially supported by Turkish Academy of Sciences (TÜBA) through the GEBİP Program.

APPENDIX: ANALYTICAL TREATMENT OF THE SYSTEM NEAR THE TRANSITION TEMPERATURE

The system analyzed in Ref. 46 is already given in Fig. 1. The approach in Ref. 46 is based on finding the point of loss of stability of the paraelectric phase for a ferroelectric slab with dead layers. While the system in Ref. 46 is treated in one half of the film with dead layers as being vacuum and the film being very thick compared to the dead layers, this approach was generalized in Ref. 47, and we follow this general approach by full treatment of the film with high-k dead layers. Going back to the system in Fig. 1, for a given dead layer thickness, d (1 $BaTiO_3$ unit cell thick, ~0.4 nm, in this work), the boundary conditions of the system can be written as

$$D_F^z - D_d^z = 0 \,@\, z = \pm L/2, \tag{A1}$$

where $D_F^z = \varepsilon_b \varepsilon_0 E_z^F + P$ and $D_d^z = \varepsilon_z^d \varepsilon_0 E_z^d$ are the dielectric displacements in the FE and dead layers, respectively, with ε_0 being the permittivity of vacuum in International system of units (SI) units, ε_z^d is the dielectric constant of the dead layer, ε_b is the background dielectric constant of the FE, P is the ferroelectric polarization in the FE along the film thickness, and L is the FE film thickness (see Fig. 1). The boundary conditions for the potential are as follows:

$$\phi_F = \phi_d @ z = \pm L/2, \tag{A2a}$$

$$\phi_d = 0 @ z = L/2 + d, \tag{A2b}$$

$$\phi_d = 0 @ z = -L/2 - d, \tag{A2c}$$

where $\phi_{F,d}$ are the potentials in the FE and the dead layer, respectively. The electric fields in the layers can then be found from the gradient of the potentials. From Eq. (1), one gets

$$-\varepsilon_b \varepsilon_0 \frac{\partial \phi_F}{\partial z} + P - \varepsilon_0 \varepsilon_z^d \frac{\partial \phi_d}{\partial z} = 0 @ z = L/2. \tag{A3}$$

In the absence of free charges, $divD = 0$ both in the FE and the dead layers. Writing these conditions in terms of the potential and polarization in the FE film, we get

$$\frac{\partial^2 \phi_F}{\partial z^2} + \frac{\varepsilon_\perp}{\varepsilon_b} \frac{\partial^2 \phi_F}{\partial x^2} = \frac{1}{\varepsilon_b \varepsilon_0} \frac{\partial P}{\partial z}, \tag{A4}$$

where $\varepsilon_\perp$ is the dielectric constant of the FE along the plane of the film (calculated as approximately 40 from the simulations, and this value is used) and

$$\varepsilon_0 \left(\varepsilon_z^P \frac{\partial^2 \phi_d}{\partial z^2} + \varepsilon_\perp^P \frac{\partial^2 \phi_d}{\partial x^2} \right) = 0 \tag{A5}$$

for the dead layer. For convenience, it is assumed that the dead layer is isotropic and $\varepsilon_z^d = \varepsilon_\perp^d$, with $\varepsilon_\perp^d$ being the dielectric constant of the dead layer along the film plane. The linear equation of state of the FE that is obtained by minimization of the Landau-Ginzburg free energy with its lowest order terms is

$$AP - g \frac{\partial^2 P}{\partial x^2} = -\frac{\partial \phi_F}{dz}, \tag{A6}$$

where the gradient of P along z has been neglected, as mentioned above, $A = (T - T_C)/\varepsilon_0 C + M$, where T is temperature, T_C is the transition temperature in bulk form, C is the Curie constant, M represents any contribution of strain in the case of a FE on a substrate (see the modified coefficient of the lowest order term in P in the free energy in Ref. 36), and g is the gradient energy coefficient. Note that the energy due to gradients along z is much less than the gradients of P along x, allowing one to safely neglect gradients along z. To solve the polarization and the potential using the differential equations above together with the equation of state in the FE, one can use the Fourier transform to express the polarization and the potentials in the layers in terms of harmonics,

$$P = \sum_k P_k e^{ikx}, \phi_F = \sum_k \phi_F^k e^{ikx}, \phi_d = \sum_k \phi_d^k e^{ikx}, \tag{A7}$$

where P_k, ϕ_F^k, and ϕ_d^k are the z-amplitudes of each harmonic in k. Inserting these Fourier transforms for a given k into Eqs. (A4), (A5), and (A6), we get

$$\frac{\partial^2 \phi_F^k}{\partial z^2} + q^2 \phi_F^k = 0, \tag{A8}$$

$$\frac{\partial^2 \phi_d^k}{\partial z^2} - k^2 \phi_d^k = 0, \tag{A9}$$

where $q = (\varepsilon_\perp \varepsilon_b \varepsilon_0 k^2 |A + gk^2|)^{1/2}$. The solutions of Eqs. (A8) and (A9) that satisfy the boundary conditions (BCs) given in Eq. (A2) are

$$\phi_F^k = A\cos qz + B\sin qz, \tag{A10}$$

$$\phi_d^k = C\sinh k(z - L - d) + D\cosh k(z - L), \tag{A11}$$

where A, B, C, and the D are the amplitudes in the general solution. Using the BCs given in Eqs. (A1) and (A2c), we get two equations with two unknowns, B and C from Eqs. (A10) and (A11),

$$B\left[q\cos\frac{qL}{2}+\frac{q}{\varepsilon_b\varepsilon_0(A+gk^2)}\cos\frac{qL}{2}\right]-\varepsilon_z^d kC\cosh-\frac{kd}{2}=0, \quad \text{(A12a)}$$

$$B\sin\frac{qL}{2}-C\sinh-\frac{kd}{2}=0. \quad \text{(A12b)}$$

For a non-trivial solution to exist, the determinants of the coefficients in Eqs. (A12a) and (A12b) have to be zero, giving us

$$B\left[\sinh\frac{kd}{2}\left(q\cos\frac{qL}{2}+\frac{q}{\varepsilon_b\varepsilon_0(A+gk^2)}\cos\frac{qL}{2}\right)+\varepsilon_z^d k\cosh-\frac{kd}{2}\sin\frac{qL}{2}\right]=0, \quad \text{(A13)}$$

meaning that

$$\sinh\frac{kd}{2}\left(q\cos\frac{qL}{2}+\frac{q}{\varepsilon_b\varepsilon_0(A+gk^2)}\cos\frac{qL}{2}\right)+\varepsilon_z^d k\cosh-\frac{kd}{2}\sin\frac{qL}{2}=0. \quad \text{(A14)}$$

After some algebra on Eq. (14), one gets

$$\tan\frac{qL}{2}=\frac{\sqrt{|\varepsilon_k|\varepsilon_\perp}}{\varepsilon_z^d}\tanh\frac{kd}{2}, \quad \text{(A15a)}$$

where

$$|\varepsilon_k|=\left(\frac{1}{\varepsilon_0(A+gk^2)}+1\right), \quad \text{(A15b)}$$

which was previously obtained by the authors of Ref. 46 through a similar route. Their approach is somewhat repeated here for tractability of results in our paper. We solve Eq. (15) using a numerical approach and seek the k value that yields the highest transition temperature from the paraelectric state into the ferroelectric state for a given d (1-unit cell-thick in this work). We do not carry out the calculations in the single domain state regime, which correspond to thicknesses smaller than 3 nm and are outside the scope of our analysis. Also note that the described method is applied for the validation of the simulation results and do not reflect any depletion charge–related effects, which are separately given only by the numerical simulation presented in this paper.

[1]S. Triebwasser, Phys. Rev. **118**, 100 (1960).
[2]A. P. Levanyuk and A. S. Sigov, "Defects and structural phase transitions," in *Ferroelectricity and Related Phenomena*, edited by W. Taylor (Gordon and Breach, New York, 1988), Vol. 6.
[3]W. L. Warren, D. Dimos, G. E. Pike, B. A. Tuttle, M. V. Raymond, R. Ramesh, and J. T. Evans, Appl. Phys. Lett. **67**, 866 (1995).
[4]T. M. Shaw, S. Troiler-McKinstry, and P. C. Mcintyre, Annu. Rev. Mater. Sci. **30**, 263 (2000).
[5]R. Ramesh, S. Aggarwal, and O. Auciello, Mater. Sci. Eng. R. **32**, 191 (2001).
[6]C. S. Ganpule, A. L. Roytburd, V. Nagarajan, B. K. Hill, S. B. Ogale, E. D. Williams, R. Ramesh, and J. F. Scott, Phys. Rev. B **65**, 014101 (2002).
[7]H. Z. Jin and J. Zhu, J. Appl. Phys. **92**, 4594 (2002).
[8]M.-W. Chu, I. Szafraniak, R. Scholz, C. Harnagea, D. Hesse, M. Alexe, and U. Gösele, Nature Mater. **3**, 87 (2004).
[9]X. Ren, Nature Mater. **3**, 91 (2004).
[10]E. Cockayne and B. P. Burton, Phys. Rev. B **69**, 144116 (2004).
[11]A. N. Morozovska and E. A. Eliseev, J. Phys: Condens. Matter **16**, 8937 (2004).
[12]D. Balzar, P. A. Ramakrishnan, and A. M. Hermann, Phys. Rev. B **70**, 092103 (2004).
[13]S. P. Alpay, I. B. Misirlioglu, V. Nagarajan, and R. Ramesh, Appl. Phys. Lett. **85**, 2044 (2004).
[14]Y. Zheng, B. Wang, and C. H. Woo, Appl. Phys. Lett. **88**, 092903 (2006).
[15]I. P. Batra and B. D. Silverman, Solid State Commun. **11**, 291 (1972).
[16]R. Kretschmer and K. Binder, Phys. Rev. B **20**, 1065 (1979).
[17]A. M. Bratkovsky and A. P. Levanyuk, Phys. Rev. Lett. **84**, 3177 (2000).
[18]J. Junquero and P. Ghosez, Nature **422**, 506 (2003).
[19]Z. Q. Wu, N. D. Huang, Z. R. Liu, J. Wu, W. H. Duan, B. L. Gu, and X. W. Zhang, Phys. Rev. B **70**, 104108 (2004).
[20]D. J. Kim, J. Y. Jo, Y. S. Kim, Y. J. Chang, J. S. Lee, J. G. Yoon, T. K. Song, and T. W. Noh, Phys. Rev. Lett. **85**, 237602 (2005).
[21]G. Gerra, A. K. Tagantsev, N. Setter, and K. Parlinski, Phys. Rev. Lett. **96**, 107603 (2006).
[22]R. Ahluwalia and D. J. Srolovitz, Phys. Rev. B **76**, 174121 (2007).
[23]A. Artemev and A. Roytburd, Acta Mater. **58**, 1004 (2010).
[24]Y. Wang, M. K. Niranjan, K. Janicka, J. P. Velev, M. Y. Zhuravlev, S. S. Jaswal, and E. Y. Tsymbal, Phys. Rev. B **82**, 094114 (2010).
[25]Y. Zheng, M. Q. Cai, and C. H. Woo, Acta Mater. **58**, 3050 (2010).
[26]M. Q. Cai, Y. Zheng, P.-W. Ma, and C. H. Woo, J. Appl. Phys. **109**, 024103 (2011).
[27]N. G. Nathaniel, R. Ahluwalia, H. B. Su, and F. Boey, Acta Mater. **57**, 2047 (2008).
[28]M. Dawber, K. M. Rabe, and J. F. Scott, Rev. Mod. Phys. **77**, 1083 (2005).
[29]A. M. Bratkovsky and A. P. Levanyuk, Phys. Rev. B. **61**, 15042 (2000). For the treatment of real electrodes, see A. M. Bratkovsky and A. P. Levanyuk, J. Comp. Theor. Nanosci., 6, 465 (2009).
[30]H. Matsuura, New J. Phys. **2**, 8 (2000).
[31]Y. Xiao, V. B. Shenoy, and K. Bhattacharya, Phys. Rev. Lett. **95**, 247603 (2005).
[32]M. B. Okatan, J. V. Mantese, and S. P. Alpay, Acta Mater. **58**, 39 (2010).
[33]Y. Zhang, J. Li, and D. Fang, Phys. Rev. B **82**, 064103 (2010).
[34]L. Hong, A. K. Soh, Q. G. Du, and J. Y. Li, Phys. Rev. B **77**, 094104 (2008).
[35]M. Dawber and J. F. Scott, Appl. Phys. Lett. **76**, 1060 (2000).
[36]L. Pintilie and M. Alexe, J. Appl. Phys. **98**, 124103 (2005).
[37]L. Pintilie, I. Boerasu, M. J. M. Gomez, T. Zhao, R. Ramesh, and M. Alexe, J. Appl. Phys. **98**, 124104 (2005).
[38]P. Zubko, D. J. Jung, and J. F. Scott, J. Appl. Phys. **100**, 114112 (2006).
[39]I. B. Misirlioglu, M. B. Okatan, and S. P. Alpay, J. Appl. Phys. **108**, 034105 (2010).
[40]M. D. Glinchuk, E. A. Eliseev, and A. N. Morozovska, Ferroelectrics **354**, 86 (2007).
[41]M. D. Glinchuk, B. Y. Zaulychny, and V. A. Stephanovich, Phys. Status Solidi **243**, 542 (2006).
[42]N. A. Pertsev, A. G. Zembilgotov, and A. K. Tagantsev, Phys. Rev. Lett. **80**, 1988 (1998).
[43]J. Hlinka and P. Marton, Phys. Rev. B **74**, 104104 (2006); A. K. Tagantsev, Ferroelectrics **375**, 19 (2008).
[44]I. B. Misirlioglu and M. Yildiz, *Proceedings of IEEE ISAF/PFM in Vancouver*, Canada, July 24–27, 2011.
[45]M. B. Okatan, A. L. Roytburd, J. V. Mantese, and S. P. Alpay, J. Appl. Phys. **105**, 114106 (2009).
[46]E. V. Chensky and V. V. Tarasenko, Sov. Phys. JETP **56**, 618 (1982); Zh. Eksp. Teor. Fiz. **83**, 1089 (1982).
[47]A. S. Sidorkin, *Domain Structure in Ferroelectrics and Related Materials* (Cambridge International Science, Moscow 2006).

Author Proof